

Collision Avoidance Strategy for the Autocrane

Dong Wang ^{1,*} , Baochang Liu ¹, Jian Shen ^{2,3,4}, Li Chen ^{2,3,4} and Lydia Zhu ⁵

¹ School of Instrument Science and Engineering, Southeast University, Nanjing 210096, China; 22017210@seu.edu.cn

² NARI Group Corporation, State Grid Electric Power Research Institute, Nanjing 211106, China; shenjian@sgepri.sgc.com.cn (J.S.); chenli1@sgepri.sgc.com.cn (L.C.)

³ NARI Technology Co., Ltd., Nanjing 211106, China

⁴ State Key Laboratory of Smart Grid Protection and Control, Nanjing 211106, China

⁵ Department of Mechanical Aerospace & Engineering, North Carolina State University, Raleigh, NC 27695, USA; Lzhu6@ncsu.edu

* Correspondence: kingeast16@seu.edu.cn

Abstract: The collision between the boom of the autocrane and the obstacle may cause serious equipment damages or casualties. With the development of 6G technology, data between multiple autocranes could be shared in real time, which makes it possible to finely control the autocranes. In order to avoid collision accidents, a collision avoidance strategy is proposed in this paper. This strategy focuses on the evaluation of the collision urgency and different evaluation methods are designed to match the three basic exercise modes of the boom. Based on the collision urgency, the control strategy is then put forward to ensure the boom's safety in every collision risk level. Additionally, two special cases are also considered to guarantee that all parts of the boom, except for the end, will not hit the obstacle. Lastly, a semi-physical testing platform is established to test the performance of the proposed collision avoidance strategy.

Keywords: collision avoidance strategy; boom control; collision urgency evaluate



Citation: Wang, D.; Liu, B.; Shen, J.; Chen, L.; Zhu, L. Collision Avoidance Strategy for the Autocrane. *Sensors* **2021**, *21*, 6746. <https://doi.org/10.3390/s21206746>

Academic Editor: Sotirios K. Goudos

Received: 19 August 2021
Accepted: 7 October 2021
Published: 11 October 2021

Publisher's Note: MDPI stays neutral with regard to jurisdictional claims in published maps and institutional affiliations.



Copyright: © 2021 by the authors. Licensee MDPI, Basel, Switzerland. This article is an open access article distributed under the terms and conditions of the Creative Commons Attribution (CC BY) license (<https://creativecommons.org/licenses/by/4.0/>).

1. Introduction

The autocrane, which is equipped with the lifting mechanism boom, is widely used for moving heavy objects in the engineering construction industry and in the working condition [1,2]. The crane operator uses a series of transmission devices to drive the boom to move in the space, thereby manipulating the hook to lift heavy objects [3,4]. However, due to the complex operating environment and the negligence of the operator, collision between the boom and the obstacle sometimes occurs. Especially when the steel boom touches the high voltage cable, the collision may result in serious personal injuries and deaths, which should be avoided as much as possible [5,6].

Researchers worldwide have developed many effective methods to make the movement of the boom smoother with easier operation and to reduce the collision risk caused by mis-operation [7–9]. Hirokazu Araya [10,11] invented a luffing follow-up control system, which could realize the horizontal movement of the hoisting load by simultaneously controlling the hoisting hoist and luffing hoist on the crawler crane. At the same time, a linear excavation control system for the hydraulic excavator was also proposed and the straight-line excavation of the bucket could be realized by controlling the boom, stick, and bucket cylinder. The Margelus company applied for a patent for the path control and vibration suppression of an articulated ladder or lifting platform. In this patent, a variety of sensors are used to collect signals and input them into the controller for calculation to improve the accuracy of the movement of a single mechanism and suppress the vibration problems during exercise. Additionally, Eckhard [12] used a non-linear control strategy to solve the radial yaw phenomenon caused by the crane in trajectory tracking. Sebastian [13] used the feedforward method to suppress the vibration caused by the single-stroke luffing

hydraulic cylinder in the horizontal crane load. Ehsan Maleki [14] used input signal-tuning to suppress the swing caused by the horizontal load of the crane. While the above methods have improved the control accuracy of the boom of the autocrane, the distance between the obstacle and the boom was not considered in any of the control strategies, which should raise the collision risk rapidly when the boom is near the obstacle [15,16].

Thus, in this paper, a two-stage collision avoidance strategy is proposed, which could limit the exercise of the boom, based on both the collision urgency and the distance to the obstacle. In this way, when the boom approaches obstacles, it will go through two processes: speed limit and being forced to stop, which make the movement of the boom smoother while ensuring safety. To identify the actual effect of the strategy, three basic movement modes of the boom are tested in the semi-physical experiments.

The remainder of this paper is organized as follows. The kinematic model of the autocrane is given in Section 2. Section 3 elaborates on the distance-based collision avoidance strategy and in this section, the strategy is divided to fit the three single movements of the boom, which are pitching, stretching, and horizontal rotation. In Section 4, a semi-physical simulation platform is built to verify the correction of the proposed collision avoidance strategy. Furthermore, the simulations and the experiments show the actual effect of the strategy. Section 5 concludes the paper.

2. Kinematic Model of the Autocrane

The concise kinematic model is essential in the formulation of the collision avoidance strategy, which is used to describe the relationship between the position of the boom and its control inputs.

2.1. Space Position of the Boom

The structure of the autocrane could be simplified as shown in Figure 1, in which the vehicle part is ignored [17]. The whole structure could rotate around point O and the lengths of D_1 and D_2 do not change in the movement of the boom. The boom of the autocrane could stretch between L_{max} and L_{min} , and pitch in the range of $\theta_{uprange} + \theta_{downrange}$. The tail end of the boom was marked with a triangle symbol. It is obvious that there are three single modes of motion for the boom, which are pitching, stretching, and horizontal rotation [18].

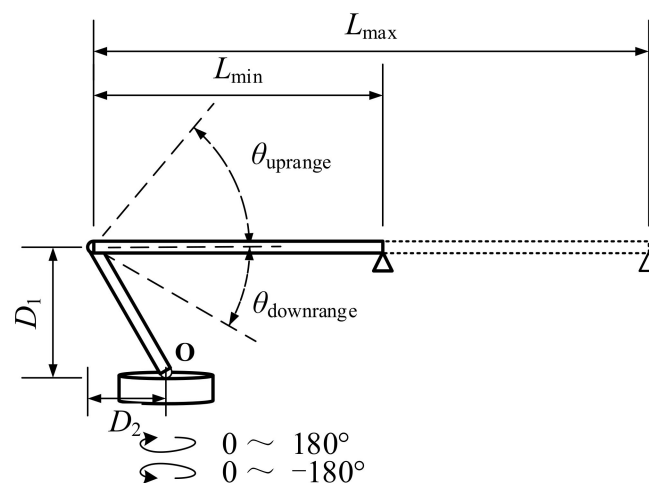


Figure 1. Structure of the autocrane.

In order to describe the relationship between the movements of the boom and its spatial position, which is a coordinate $(Oxyz)$, is formulated in Figure 2. O is fixed at the center of the rotation. The axis Oz is positioned vertically upwards and coincides with the rotation axis. The axis Ox is positioned towards the head of the autocrane and the axis Oy is positioned to the side to constitute a right-handed coordinate. In this way, the position

of the boom could be completely determined by the coordinates of points O' and P , which are the two end points of the boom, as shown in Equations (1) and (2).

$$O'(x'_O, y'_O, z'_O) : \begin{cases} x'_O = -D_2 * \cos \omega \\ y'_O = -D_2 * \sin \omega \\ z'_O = D_1 \end{cases} \quad (1)$$

$$P(x_p, y_p, z_p) : \begin{cases} x_p = (L * \cos \theta - D_2) * \cos \omega \\ y_p = (L * \cos \theta - D_2) * \sin \omega \\ z_p = L * \sin \theta + D_1 \end{cases} \quad (2)$$

where L ($L_{min} \leq L \leq L_{max}$) is the length of the boom. θ ($-\theta_{downrange} \leq \theta \leq \theta_{uprange}$) is the pitch angle of the boom and is defined as positive when positioned upwards. ω ($-180^\circ \leq \omega \leq 180^\circ$) is the horizontal rotational angle of the boom and the positive direction is defined in the counterclockwise direction. The above three parameters are the control amount inputs of the boom and could make the boom stretch, pitch, and horizontally rotate, respectively.

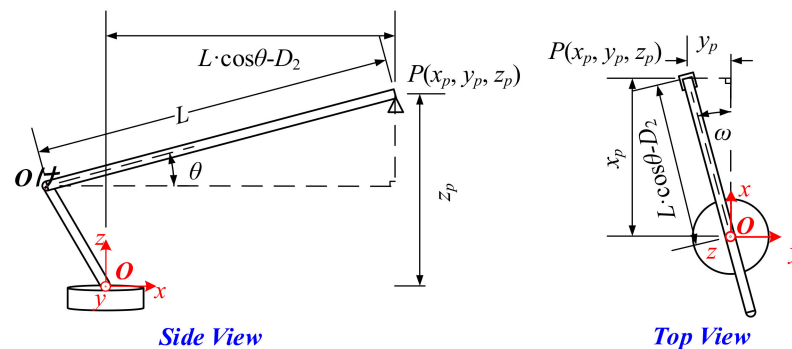


Figure 2. Relationship between the movement of the boom and its spatial position.

2.2. Space Position of the Obstacle

The detection of the obstacle was the premise of collision avoidance. For instance, take the high voltage cable as an example: the available sensors include one or more cameras, an electric field sensor, a millimeter wave radar, and LIDAR [19,20]. These sensors are always fixed on the tail end of the boom for convenience and could obtain the relative position between the boom and obstacle [21], as shown in Figure 3.

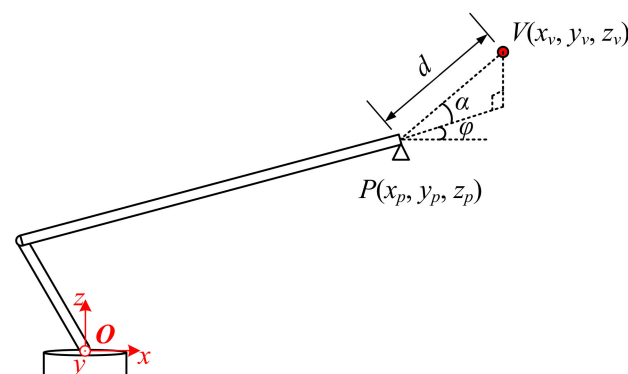


Figure 3. Relative position between the boom and obstacle.

Where d is the length of line segment PV , α and φ are the pitch angle and heading angle of line segment PV in the coordinate $Oxyz$. The above parameters (d , α , and φ) could fully describe the relative position between the boom and the obstacle. In this case, the

space position of the obstacle $V(a', b', c')$ in the coordinate $Oxyz$ is obvious, as shown in Equation (3).

$$V(x_v, y_v, z_v) : \begin{cases} x_v = x_p + d * \cos \alpha * \cos \varphi \\ y_v = y_p + d * \cos \alpha * \sin \varphi \\ z_v = z_p + d * \sin \alpha \end{cases} \quad (3)$$

3. Collision Avoidance Strategy

The collision avoidance strategy in this paper is based on both the safety range and the collision urgency. Firstly, a safety radius R is defined around the obstacle and the boom is not allowed to enter the range of the radius, which means the boom must stop moving forward and only allow for only moving backwards when the distance to the obstacle (d in Figure 3) is less than or equal to the safety radius R [22,23]. Secondly, considering that the emergency brake easily causes damage to the boom actuator, a hierarchical control method depending on the collision urgency was designed to make the boom move more smoothly. The collision urgency was evaluated by the time T for the boom to reach the safety range, which is defined in Equation (4). It is worth noting that v_c is not the real speed of the boom but rather is the speed corresponding to the operator's input. When T is greater than threshold T_0 , which means there is no collision in the near future, the boom is directly controlled by the operator of the autocrane. As long as the detecting T is less than T_0 , meaning the boom has a higher risk of collision, the control value input by the operator will be multiplied by the coefficient ρ ($0 < \rho < 1$) before being sent to the boom controller. Figure 4 explains the above strategy. In taking the three movement modes of the boom into account, the specific calculation methods of the parameter T are different, which will be illustrated in the rest of this section.

$$T = \frac{d - R}{v_c} \quad (4)$$

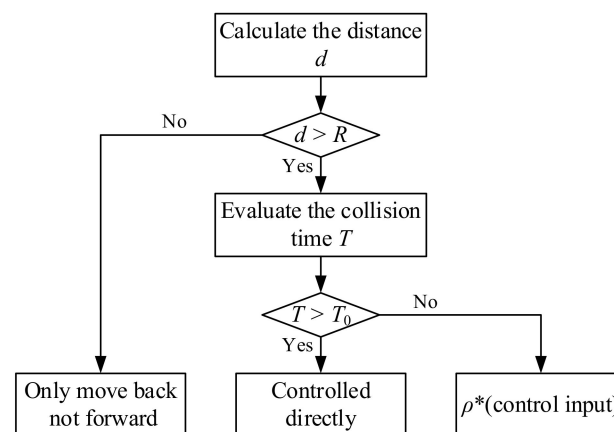


Figure 4. Collision avoidance strategy.

Figure 5 shows how the collision avoidance strategy improves the traditional boom control method. In the traditional strategy, the operator controls the boom directly through the crane's controller, thus, if the operator does not take braking measures, there is a risk of the boom colliding with obstacles. However, in this paper, the proposed strategy determines whether the operator's control input is directly proportional or otherwise will stop moving forward, as delivered to the controller according to the calculation of T and d . This means that the operator can control the boom in any way and the boom will not collide with obstacles.

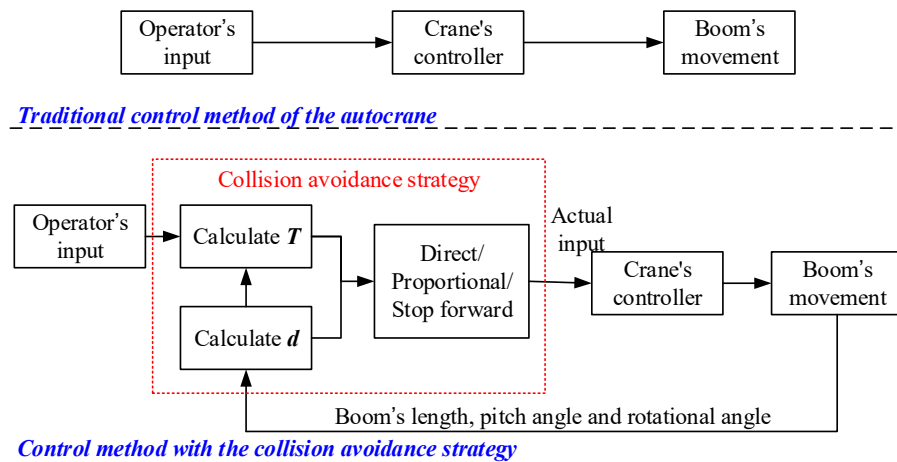


Figure 5. Control method with and without the collision avoidance strategy.

3.1. Collision Urgency Evaluation for Stretching

As shown in Figure 6, the boom could only stretch in this situation. It is obvious that the end of the boom is not allowed to break through the surface of the safety sphere, thus the collision condition can be described as in Equation (5). When the boom is stretching at a constant speed V_L , the coordinates of point P' could be provided, as in Equation (6).

$$(x_v - x_{p'})^2 + (y_v - y_{p'})^2 + (z_v - z_{p'})^2 = R^2 \quad (5)$$

$$\begin{cases} x_{p'} = x_p + V_L T \cos \theta * \cos \omega \\ y_{p'} = y_p + V_L T \cos \theta * \sin \omega \\ z_{p'} = z_p + V_L T \sin \theta \end{cases} \quad (6)$$

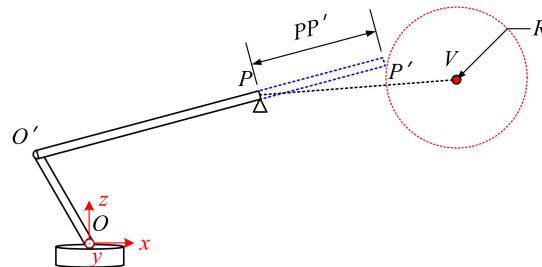


Figure 6. Collision urgency evaluation for stretching.

Substitute Equation (6) into Equation (5): the parameter T , which represents the collision urgency, could be obtained by solving a quadratic equation in one variable. Although the equation supports having two solutions for entering and leaving the safety range, T is obviously corresponding to the entry point P' .

3.2. Collision Urgency Evaluation for Pitching

Figure 7 shows the possible collision situation in the pitching of the boom. As in the stretching, when a collision occurs, the relationship between P' and V still satisfies Equation (5). In this case, however, the coordinate of P' should be described in Equation (7).

$$\begin{cases} x_{p'} = [L * \cos(\theta + V_\theta T) - D_2] * \cos \omega \\ y_{p'} = [L * \cos(\theta + V_\theta T) - D_2] * \sin \omega \\ z_{p'} = L * \sin(\theta + V_\theta T) + D_1 \end{cases} \quad (7)$$

where V_θ is the pitch rate of the boom, which satisfies $\Delta\theta = V_\theta T$. Additionally, the estimated collision time T could be calculated by solving Equations (5) and (7).

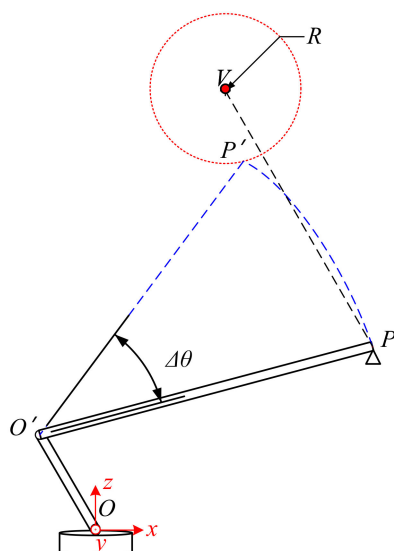


Figure 7. Collision urgency evaluation for pitching.

3.3. Collision Urgency Evaluation for Horizontal Rotation

The situation of the horizontal rotation of the boom is shown in Figure 8. When the end of the boom touches the surface of the safety sphere, the coordinate of point P' is provided, as in Equation (8).

$$\begin{cases} x_{p'} = (L * \cos \theta - D_2) * \cos(\omega + V_\omega T) \\ y_{p'} = (L * \cos \theta - D_2) * \sin(\omega + V_\omega T) \\ z_{p'} = L * \sin \theta + D_1 \end{cases} \quad (8)$$

where V_ω is the rotational speed of the boom, which satisfies $\Delta\omega = V_\omega T$. In this way, the time T could be obtained from Equations (5) and (8).

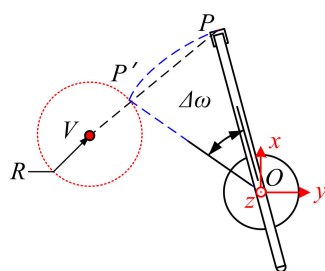


Figure 8. Collision urgency evaluation for horizontal rotation.

3.4. Special Cases

In addition to the above three cases, it is worth noting that the end of the boom is not the only place where it may collide with obstacles. When the boom is pitching or rotating horizontally, the middle of the boom might be the first to enter the range of the safety sphere, as shown in Figure 9. Under this circumstance, the collision point could be any part of the boom, thus the distance D' from point V to a straight line $O'P$ in space should be checked.

Specifically, for Figure 9a, since the boom engages in a pitching motion, the point O' does not move and the line of the boom could be described as in Equation (9).

$$\frac{x - x'_O}{X_a} = \frac{y - y'_O}{Y_a} = \frac{z - z'_O}{Z_a} \quad (9)$$

where $[X_a, Y_a, Z_a]'$ is the direction vector of the boom, which satisfies Equation (10).

$$\begin{cases} X_a = L * \cos(\theta + V_\theta T) * \cos \omega \\ Y_a = L * \cos(\theta + V_\theta T) * \sin \omega \\ Z_a = L * \sin(\theta + V_\theta T) \end{cases} \quad (10)$$

When the boom reaches the safety sphere, D' equals to R , as in Equation (11).

$$D' = \frac{\sqrt{\left| \begin{array}{cc} y_v - y'_O & z_v - z'_O \\ Y_a & Z_a \end{array} \right|^2 + \left| \begin{array}{cc} z_v - z'_O & x_v - x'_O \\ Z_a & X_a \end{array} \right|^2 + \left| \begin{array}{cc} x_v - x'_O & y_v - y'_O \\ X_a & Y_a \end{array} \right|^2}}{\sqrt{X_a^2 + Y_a^2 + Z_a^2}} = R \quad (11)$$

The estimated collision time T could be calculated by Equations (10) and (11).

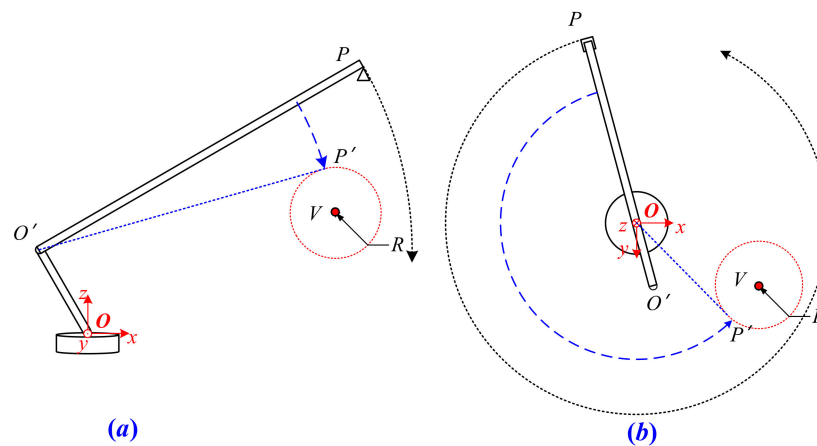


Figure 9. Collision urgency evaluation for special cases: (a) special pitching cases, (b) special rotating cases.

Similarly, for Figure 9b, the fixed-point O_b in rotating motion is the intersection point of the boom and axis Oz , and the coordinate of this point is shown in Equation (12). The straight line in the space where the boom is located can be expressed as Equation (13).

$$\begin{cases} x_{Ob} = 0 \\ y_{Ob} = 0 \\ z_{Ob} = D_1 + D_2 \tan \theta \end{cases} \quad (12)$$

$$\frac{x - x_{Ob}}{X_b} = \frac{y - y_{Ob}}{Y_b} = \frac{z - z_{Ob}}{Z_b} \quad (13)$$

where $[X_b, Y_b, Z_b]'$ is the direction vector of the boom, which satisfies Equation (14).

$$\begin{cases} X_a = (L * \cos \theta - D_2) * \cos(\omega + V_\omega T) \\ Y_a = (L * \cos \theta - D_2) * \sin(\omega + V_\omega T) \\ Z_a = L * \sin \theta - D_2 \tan \theta \end{cases} \quad (14)$$

In this case, when the boom reaches the safety sphere, D' equals to R , as in Equation (15).

$$D' = \frac{\sqrt{\left| \begin{array}{cc} y_v - y_{Ob} & z_v - z_{Ob} \\ Y_b & Z_b \end{array} \right|^2 + \left| \begin{array}{cc} z_v - z_{Ob} & x_v - x_{Ob} \\ Z_b & X_b \end{array} \right|^2 + \left| \begin{array}{cc} x_v - x_{Ob} & y_v - y_{Ob} \\ X_b & Y_b \end{array} \right|^2}}{\sqrt{X_b^2 + Y_b^2 + Z_b^2}} = R \quad (15)$$

Additionally, time T could be obtained by Equations (14) and (15).

4. Semi-Physical Experiments

In order to test the performance of the proposed collision avoidance strategy, a semi-physical testing platform was established, as shown in Figure 10. The electric control boom model, which has three movable degrees of freedom (pitching, stretching, and horizontal rotation) was used to simulate the real boom on the autocrane. Its movement was controlled by the PLC controller. The sensors on the model contribute the spatial location of the boom. The pull-wire displacement sensor fixed on the end of the boom could measure the length of the boom (L). At the same time, the IMU gave the pitching and rotational angle (θ and ω) of the boom. Additionally, the horizontal position and height of the obstacle could be adjusted by the fixed bracket and support rod.

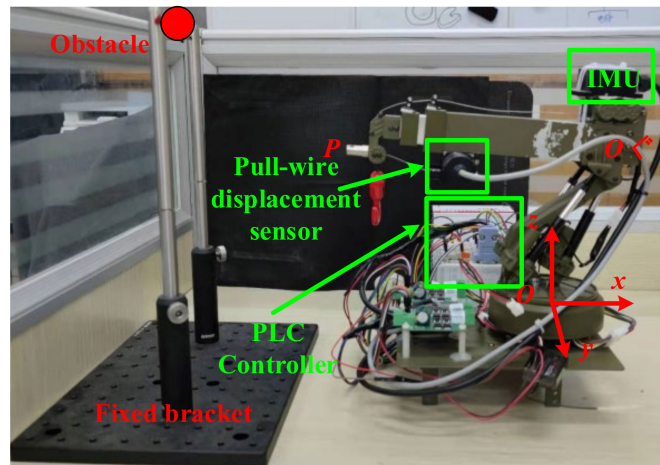


Figure 10. Semi-physical testing platform.

In this testing platform, some of the structural parameters could be determined before the experiments. Specifically, $D_1 = 130$ mm, $D_2 = 67.5$ mm, $L_{max} = 462$ mm, $L_{min} = 240$ mm, $\theta_{uprange} = 50^\circ$, and $\theta_{downrange} = 30^\circ$.

Furthermore, the parameters for the collision avoidance strategy were also set, such as the safety radius $R = 50$ mm, collision time threshold $T_0 = 5$ s, and control coefficient $\rho = 0.3$. Under the above premises, the stretching, pitching, and rotation tests were carried out.

4.1. Stretching Test

In the stretching test, the location of the obstacle in coordinate $Oxyz$ was set as (273, 0, 130) and $Oxyz$ had a unit length of 1 mm. The initial states of the boom were $L = 240$ mm, $\theta = 0^\circ$, $\omega = 0^\circ$. It is supposed that the operator controls the boom to extend at a constant speed and both the real change of the boom length and the distance to the obstacle are shown in Figure 11.

In Figure 11, the solid and dashed lines represent different original extending speeds, which are 2.23 mm/s for the solid line and 1.65 mm/s for the dashed line. By comparing the time and position of the boom when entering the control intervention phase, it can be found that at different initial speeds, the collision urgency time T of the proportional control stage (rose dotted line) and the distance to the obstacle of the forward limit stage (orange dotted line) were always the same, which is consistent with the strategy design.

4.2. Pitching and Rotating Test

The initial parameters in the pitching test were set as $V(180, 0, 180)$, $L = 240$ mm, $\theta = 60^\circ$, and $\omega = 0^\circ$, and for the rotating test, $V(180, 50, 130)$, $L = 240$ mm, $\theta = 0^\circ$, and $\omega = -63^\circ$. The testing results are shown in Figure 12a,b. It is obvious that under the proposed collision avoidance strategy, both the pitching rate and the rotational speed of the boom started to decelerate when the collision urgency time T was less than 5 s (rose dotted line) and it was not allowed to move forward when the end of the boom touched

the surface of the safety sphere, which means that its distance to the obstacle equaled to 50 mm (orange dotted line).

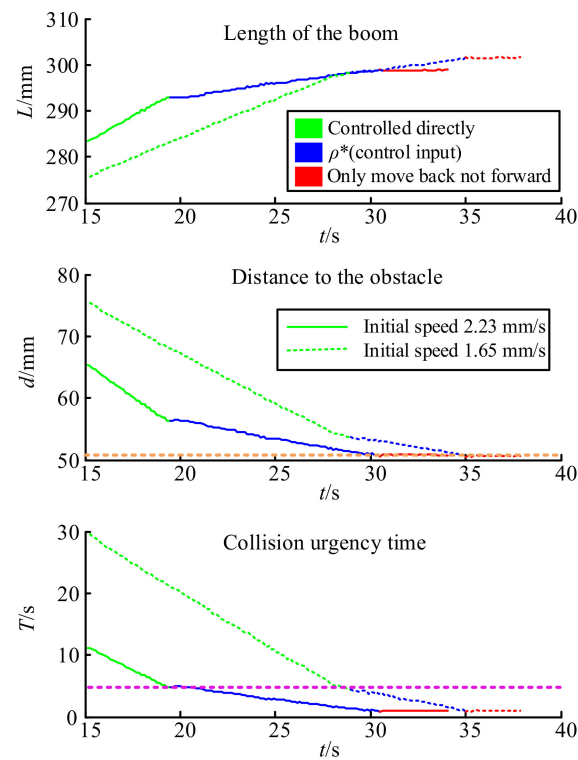


Figure 11. Result of the stretching test.

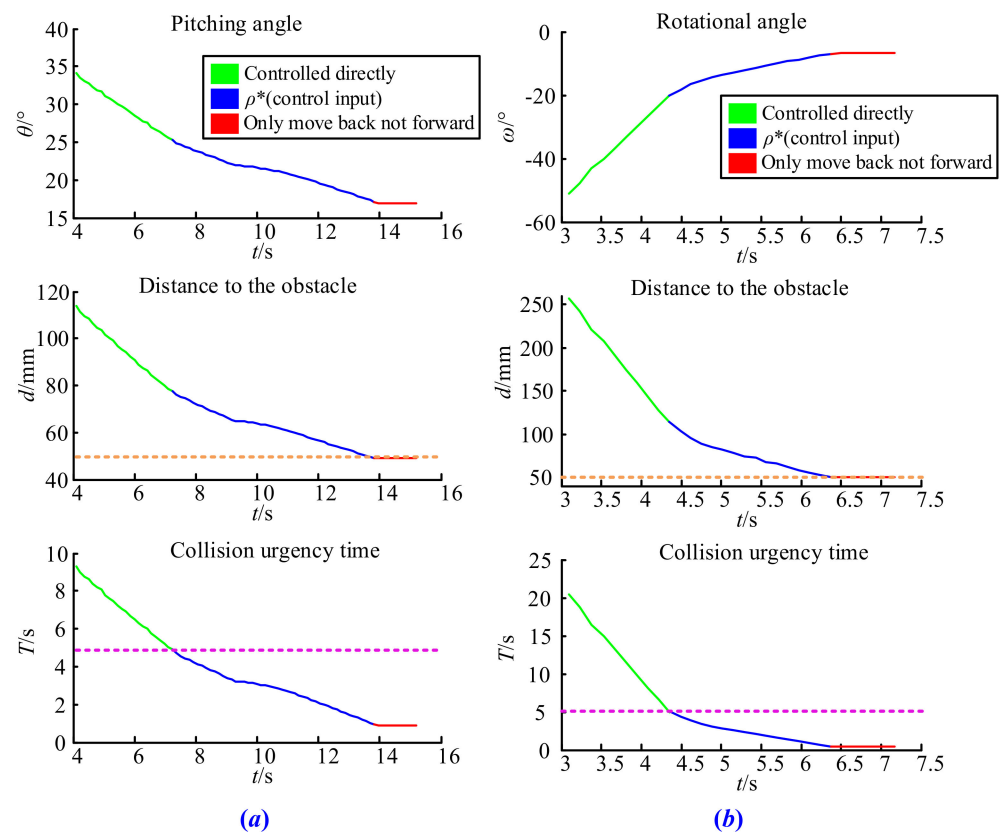


Figure 12. Result of the pitching and rotating test: (a) pitching test, (b) rotating test.

4.3. Special Case Test

When the boom is pitching, if the length of vector $O'V$ is less than the length of vector $O'P$, it belongs to the special case discussed earlier. Similarly, when the projection length of vector OV in the horizontal plane is less than that of vector OP , the end of the boom does not easily collide with obstacles, either. Under these special cases, the time T represents the shortest time for collision with obstacles at any position of the boom.

In order to complete this test, we set $V(180, 0, 180)$, $L = 350$ mm, $\theta = 48^\circ$, and $\omega = 0^\circ$ in the pitching test, and $V(180, 50, 130)$, $L = 350$ mm, $\theta = 0^\circ$, and $\omega = 110^\circ$ in the rotating test. The results shown in Figure 13a,b once again verify the effectiveness of the collision avoidance strategy proposed in this paper. It is easy to observe that the strategy begins to work when the shortest collision time between the boom and the obstacle equals to threshold T_0 , and the distance from P to the obstacle never reaches the safety sphere in the whole process. This is because P is not the closest point from the boom to the obstacle. If the strategy only considers the distance between the end of the boom and the obstacle, it may still lead to a collision accident. However, after introducing special circumstances, the collision avoidance strategy guarantees that the arbitrary movement of the boom is safe.

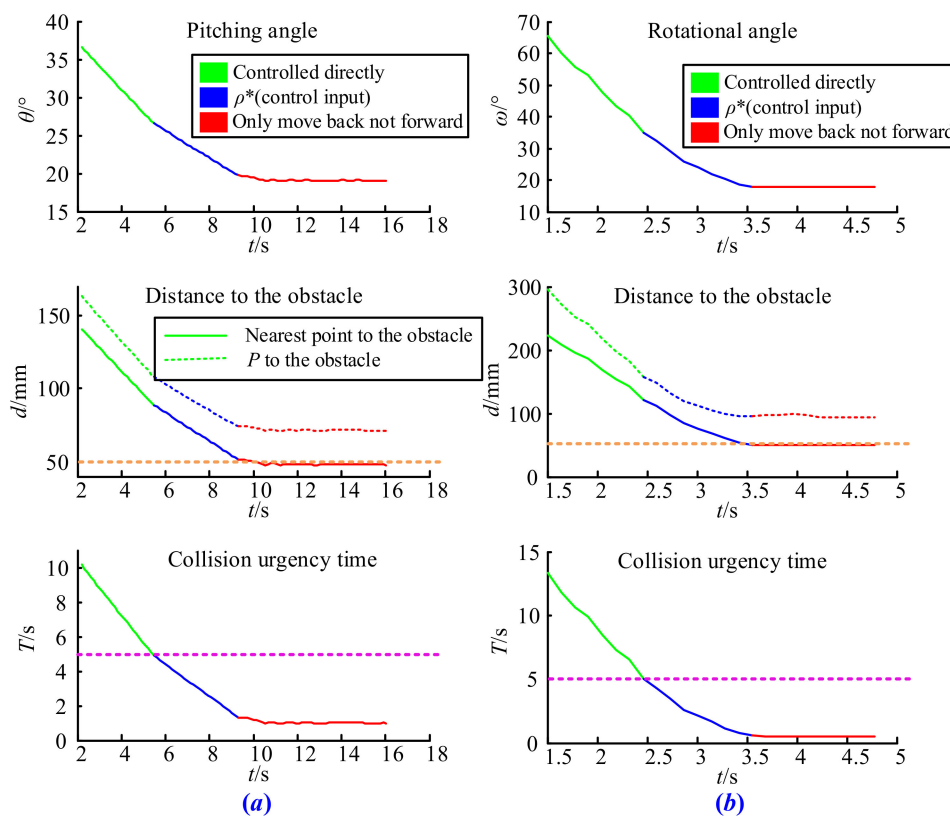


Figure 13. Result of the special case test: (a) special pitching cases, (b) special rotating cases.

5. Conclusions

In order to avoid safety accidents caused by the collision of the autocrane boom with obstacles, a collision avoidance strategy was proposed in this paper. In this strategy, both the prediction collision time and the distance to the obstacle were calculating during the movements of the boom. Based on the time and distance threshold, the movement of the boom was divided into three modes according to the urgency of the collision, which include direct control, proportional control, and the restricted approach, respectively. Additionally, the two kinds of special cases were considered to ensure that no part of the boom will break through the set security boundaries. The results of the semi-physical experiments demonstrate the correction of the collision avoidance strategy.

Author Contributions: Methodology, D.W. and B.L.; Validation, B.L.; Writing—original draft preparation, D.W.; Project Administration, J.S. and L.C.; Supervision, L.Z. All authors have read and agreed to the published version of the manuscript.

Funding: This research study was funded by the Suzhou Key Industrial Technology Innovation project, grant number SYG202031.

Institutional Review Board Statement: Not applicable.

Informed Consent Statement: Not applicable.

Data Availability Statement: Not applicable.

Acknowledgments: The authors acknowledge Min Zhang and Zuodong Xiao for their contributions in the process of equipment debugging and field testing.

Conflicts of Interest: The authors declare that they have no conflict of interest to report regarding the present study.

References

1. Ouyang, H.; Uchiyama, N.; Sano, S. Anti-sway control of rotary crane only by horizontal boom motion. In Proceedings of the 2010 IEEE International Conference on Control Applications, Yokohama, Japan, 8–10 September 2010; pp. 591–595.
2. Teng, R.M.; Wang, X.; Wang, J.Z.; Liang, J.F. Research on Vibration Suppression for Boom Luffing of Telescopic Boom Aerial Work Platform. In Proceedings of the 2018 Intelligent Computing and Internet of Things, Chongqing, China, 21–23 September 2018; pp. 330–341.
3. Yang, T.; Sun, N.; Chen, H.; Fang, Y. Motion trajectory-based transportation control for 3-D boom cranes: Analysis, design, and experiments. *IEEE Trans. Ind. Electron.* **2018**, *66*, 3636–3646. [[CrossRef](#)]
4. Uchiyama, N.; Ouyang, H.; Sano, S. Residual load sway suppression for rotary cranes using only S-curve boom horizontal motion. In Proceedings of the 2012 American Control Conference, Montréal, QC, Canada, 27–29 June 2012; pp. 6258–6263.
5. Inukai, T.; Yoshida, Y. Control of a boom crane using installed stereo vision. In Proceedings of the 2012 6th International Conference on Sensing Technology (ICST), Kolkata, India, 18–21 December 2012; pp. 189–194.
6. Koc, C.; Keskin, R. Developing of PIC controlled active boom suspension system for field sprayer. *J. Agric. Sci.* **2011**, *17*, 24–33.
7. Lian, J.; Li, J. Crane basic boom static analysis based on ANSYS. *Adv. Mater. Res.* **2014**, *871*, 64–68. [[CrossRef](#)]
8. Zeng, W.; Peng, J.; Ren, H.; Fu, L.; Liu, Y. Research on Telescopic Time-variation Dynamic Characteristics of Box-type Boom. *China Mech. Eng.* **2016**, *27*, 51–57.
9. Qin, J.; Shao, T.; Chen, J.; Wan, J.; Li, Z.; Jiang, M. Stress Analysis of Boom of Special Mobile Crane for Plain Region in Transmission Line. In Proceedings of the 2017 IOP Conference Series: Materials Science and Engineering, Bangkok, Thailand, 21–23 April 2017; pp. 1–6.
10. Araya, H.; Kakuzen, M.; Kinugawa, H.; Arai, T. Level luffing control system for crawler cranes. *Autom. Constr.* **2004**, *13*, 689–697. [[CrossRef](#)]
11. Araya, H.; Kagoshima, M. Semi-automatic control system for hydraulic shovel. *Autom. Constr.* **2001**, *10*, 477–486. [[CrossRef](#)]
12. Arnold, E.; Neupert, J.; Sawodny, O.; Schneider, K. Trajectory tracking for boom cranes based on nonlinear control and optimal trajectory generation. In Proceedings of the 2007 IEEE International Conference on Control Applications, Singapore, 1–3 October 2007; pp. 1444–1449.
13. Maleki, E.; Singhose, W.; Srinivasan, S. Positioning and control of boom crane luffing with double-pendulum payloads. In Proceedings of the 2010 IEEE International Conference on Control Applications, Yokohama, Japan, 8–10 September 2010; pp. 1319–1324.
14. Kuchler, S.; Sawodny, O.; Schneider, K.; Langer, K. Vibration damping for a hydraulic driven luffing cylinder at a boom crane using feedforward control. In Proceedings of the 2009 IEEE/ASME International Conference on Advanced Intelligent Mechatronics, Singapore, 14–17 July 2009; pp. 1276–1281.
15. Wu, W.; Yang, H.; Li, Q.; Chew, D. An integrated information management model for proactive prevention of struck-by-falling-object accidents on construction sites. *Autom. Constr.* **2013**, *34*, 67–74. [[CrossRef](#)]
16. Hayward, V.; Aubry, S.; Foisy, A.; Ghallab, Y. Efficient collision prediction among many moving objects. *Int. J. Robot. Res.* **1995**, *14*, 129–143. [[CrossRef](#)]
17. Wan, S.; Ding, S.; Chen, C. Edge Computing Enabled Video Segmentation for Real-Time Traffic Monitoring in Internet of Vehicles. *Pattern Recognit.* **2021**, *121*, 108146. [[CrossRef](#)]
18. Chen, C.; Zhang, Y.; Khosravi, M.R.; Pei, Q.; Wan, S. An intelligent platooning algorithm for sustainable transportation systems in smart cities. *IEEE Sens. J.* **2020**, *21*, 15437–15447. [[CrossRef](#)]
19. Wan, S.; Gu, Z.; Ni, Q. Cognitive computing and wireless communications on the edge for healthcare service robots. *Comput. Commun.* **2020**, *149*, 99–106. [[CrossRef](#)]
20. Gao, Z.; Xuan, H.Z.; Zhang, H.; Wan, S.; Choo, K.K.R. Adaptive fusion and category-level dictionary learning model for multiview human action recognition. *IEEE Internet Things J.* **2019**, *6*, 9280–9293. [[CrossRef](#)]

21. Xu, X.; Xue, Y.; Qi, L.; Yuan, Y.; Zhang, X.; Umer, T.; Wan, S. An edge computing-enabled computation offloading method with privacy preservation for internet of connected vehicles. *Future Gener. Comput. Syst.* **2019**, *96*, 89–100. [[CrossRef](#)]
22. Zhu, L.; Wang, Y.; Wu, Z. An Adaptive Priority Allocation for Formation UAVs in Complex Context. *IEEE Trans. Aerosp. Electron. Syst.* **2020**, *57*, 1002–1015. [[CrossRef](#)]
23. Zhu, L.; Wu, Z.; Wang, L.; Wang, Y. The identification of the wind parameters based on the interactive multi-models. *Comput. Mater. Contin.* **2020**, *65*, 405–418.